On the other hand, predictions based on the redox potentials of the phthalocyanines determined in DMA do not work very well. For example, AlClPc, TiOPc, and H_2Pc would be expected to sensitize the oxidation of Cl^-, Br^-, and H_2O based on the MPc/MPc^+ potential but they did not.

Cathodic Photocurrent. A mechanism for the anodic and cathodic photocurrents on H_2Pc-coated semiconductor electrodes has been proposed in a previous paper,[18] and will not be repeated here. The reduction of an oxidizing species in the solution by photogenerated electrons occurs only when their potentials are more negative than the V° of the redox species and the potential of the electrode is sufficiently negative to force these electrons to the solution interface. The surface electron affinities of all phthalocyanines used in this study are negative enough to supply electrons via illumination to reduce the oxidizing agents listed in Table II (Fe(III)-EDTA, BQ, O_2). Nonselective reduction, as expected, was observed. Note, however, that the energetically possible reduction of protons to H_2 did not take place, probably because the overall reaction is slow. Most p-type semiconductors, e.g., p-GaAs, are not good H_2-generation electrodes.[19]

Action Spectra and Dependence of the Sensitized Photocurrent on Light Intensity. The linear dependence of the sensitized photocurrent on the incident light intensity, I_0, implies that the sensitized photocurrent is proportional to the total rate of production of charge carriers G. The expected spectral shapes can be estimated from absorption data. The rate of carrier generation as a function of distance, x, from the illuminated surface is proportional to $\alpha \exp(-\alpha x)$, where α is the absorption coefficient of the phthalocyanine thin film. Since the film thickness, 100-250 Å, is of the order of the width of the space charge layer of the phthalocyanine thin film,[14b,c] it is assumed that the space charge layer in phthalocyanine extends the whole film thickness. The total rate of carrier production, G, is thus given by

$$G = \phi \int_0^d I_0 \alpha \exp(-\alpha x)\, dx = \phi I_0[1 - \exp(-\alpha d)] \quad (1)$$

where d is the film thickness and ϕ is the quantum efficiency of carrier generation. Because the film thickness is much smaller than the optical penetration depth (for example, even at maximal absorption, only ~15% of incident light was absorbed by the film), eq 1 can be reduced to

$$G \simeq \phi I_0 \alpha d = \phi I_0 A \quad (2)$$

or

$$G/I_0 \simeq \Phi A \quad (3)$$

where A is the absorbance of thin phthalocyanine films. Thus, if G is normalized to the same incident light intensity at every wavelength, the action spectra of the sensitized photocurrent will be expected to correspond to the absorption spectra. This is observed, at least for the general shapes, for both anodic and cathodic photocurrents.

Conclusion

The foregoing discussion shows that the surface ionization potentials, I_s, of the phthalocyanine thin films rather than the oxidation potentials of phthalocyanines in solution determine the actual oxidizing power of the photoexcited phthalocyanine molecules. Thus, attempts at using different central metal ions or changes in valency to shift I_s to more positive values for the sensitized photooxidation of H_2O, Br^-, and Cl^- seem rather unpromising; the I_s values are rather insensitive to these parameters.

An alternative approach is to modify the phthalocyanine ring by electron-withdrawing substituents and this is now under investigation. As found in previous studies with phthalocyanine materials[14,18] the quantum efficiencies for conversion of absorbed radiation to external current flow are rather low, probably because of inefficient production or rapid recombination of the charge carriers. The utilization of MPc sensitization in practical devices will require significant improvements in these quantum efficiencies.

Acknowledgments. The support of this research, which is a joint project with Professor A. B. P. Lever of York University, by the Office of Naval Research is gratefully acknowledged.

Semiconductor Electrodes. 31. Photoelectrochemistry and Photovoltaic Systems with n- and p-Type WSe_2 in Aqueous Solution

Fu-Ren F. Fan, Henry S. White, Bob L. Wheeler, and Allen J. Bard*

Contribution from the Department of Chemistry, The University of Texas at Austin, Austin, Texas 78712. *Received January 2, 1980*

Abstract: The photoelectrochemical (PEC) behavior of n- and p-type WSe_2 single crystal electrodes in aqueous solutions containing a number of redox couples (Br_2/Br^-, Fe^{3+}/Fe^{2+}, I_2/I^-, $Fe(CN)_6^{3-}/Fe(CN)_6^{4-}$, and MV^{2+}/MV^+, where MV is methylviologen) was investigated. The results are consistent with a model of the interface where ideal behavior is approached with some couples but recombination effects are important with others. The characteristics of several PEC cells are described. The n-WSe_2/I_3^- (0.025 M),I^- (1.0 M)/Pt cell showed a 0.71-V open circuit voltage, 65 mA/cm^2 short circuit current, 0.46 fill factor, and ~14% power efficiency under 150 mW/cm^2 red light irradiation. A rechargeable PEC cell based on the p-$WSe_2/MV^{2+},I^-$/n-WSe_2 system was constructed. Photoproduction of H_2 and I_2 with such a cell is also described.

Introduction

The application of semiconductor electrodes to the construction of photoelectrochemical (PEC) photovoltaic and electrophotosynthetic cells has been reviewed recently.[1] In addition to fundamental studies of the semiconductor/solution interface, investigations of such electrodes are concerned with the construction of efficient systems for the utilization of solar energy to produce electricity or chemical species. The practical application of such devices depends upon the discovery of inexpensive and abundant materials with an energy gap which matches the solar spectrum and which are capable of stable operation in solution over an extended period. This has led to the investigation of a number

(1) (a) Bard, A. J. *J. Photochem.* **1979**, *10*, 59. (b) *Science*, **1980**, *207*, 139. (c) Wrighton, M. S. *Acc. Chem. Res.* **1979**, *12*, 303. (d) Nozik, A. J. *Annu. Rev. Phys. Chem.* **1978**, *29*, 189.

0002-7863/80/1502-5142$01.00/0

of new semiconductor materials.

Recently, Tributsch and co-workers[2a-e] have described PEC cells based on layer-type semiconductors (e.g., MoS_2 and $MoSe_2$) which show reasonable efficiencies and good stability in aqueous solutions. In recent work, cells based on p-WSe_2,[3] as well as the dependence of the photopotential on the solution redox couple for n-WSe_2,[4] have been discussed. Wrighton and co-workers have recently reported that $MoSe_2$ shows high efficiency and good stability in acetonitrile medium containing Cl^-/Cl_2.[2f] Since these layer compounds appear to be promising materials for practical applications, we have initiated an investigation of their electrochemical behavior in aqueous and nonaqueous solutions. In this paper we describe experiments with n- and p-type WSe_2 and demonstrate that rather efficient photovoltaic cells can be constructed with these materials. The application of the p-WSe_2/methylviologen system to the photogeneration of hydrogen will be discussed. Finally a rechargeable photoredox cell, based on the dual photocell concept[1a,5] and employing both n- and p-WSe_2 with an aqueous methylviologen iodide solution, will be described.

Experimental Section

The semiconductors used were n- and p-type WSe_2 single crystals generously donated by Drs. Barry Miller and Frank DiSalvo, Bell Laboratories. They were electrically contacted to a copper wire by means of conductive silver epoxy cement (Allied Products Corp., New Haven, Conn.) which was subsequently covered with 5-min epoxy cement. Before the crystal was mounted, a clean, new crystal surface ($\perp$ c axis) was prepared by sticking adhesive tape on it and then pulling it, along with a surface layer of the crystal, off. The semiconductor material was then mounted into 7-mm-diameter glass tubing. The electrode was covered, along with the copper wire and all sides of the crystal, except for the newly formed van der Waals surface ($\perp$ c axis), with silicone rubber sealant (Dow Corning Corp., Midland, Mich.). The exposed area of p-WSe_2 was 0.055 cm^2 and that of n-WSe_2 0.017 cm^2. The geometric area of the n-WSe_2 electrode measured optically agrees within 10% with the area determined by comparing the cathodic peak currents for the reduction of methyl- or heptylviologen on this n-WSe_2 electrode to those of a platinum disk electrode of known geometric area. The behavior of WSe_2 electrodes depends critically on the nature of the surface and characteristics of the crystal used. Those employed in these studies were carefully selected by microscopic examination to find ones which had no pits, edges, or other crystal imperfections on the electrode surface. Such electrodes showed no dispersion in capacitance (C) over a range of frequencies of 100 Hz to 10 kHz and showed linear $1/C^2$ vs. potential (Mott-Schottky) plots over a range of 0.8 V; these results will be described in detail elsewhere. Before use, the surface of the electrode was etched with 12 M HCl for 5–10 s and then rinsed thoroughly with water.

A conventional three-electrode, single-compartment cell was used for the electrochemical measurements, unless noted otherwise. The electrochemical cell (volume ~25 mL) which contained the Pt disk, Au foil, or semiconductor working electrode was fitted with a flat Pyrex window for illumination of the semiconductor electrode. A platinum foil (~40 cm^2) was used as the counterelectrode and an aqueous saturated calomel electrode (SCE) as the reference electrode.

The cyclic voltammograms were obtained with a Princeton Applied Research (PAR) Model 173 potentiostat, PAR Model 175 universal programmer, and PAR Model 179 current-to-voltage converter and recorded on a Houston Instruments (Austin, Texas) Model 2000 X-Y recorder. In the solar cell measurements, current (i) and voltage (V) readings were taken between the working electrode and the counterelectrode or between two photoelectrodes with no external power source. The photovoltage and the photocurrent as functions of the load resistance were measured with a custom-built voltage follower and a current-to-voltage converter or with a Keithley Model 179 TRMS digital multimeter.

The light sources used in the study of the PEC effect were an Oriel Corp. (Stamford, Conn.) 450-W Xe lamp and a 1.6-mW Spectra Physics Model 132 He–Ne laser. Experiments designed for specific wavelengths employed an Oriel 7240 grating monochromator with a 20-nm band-pass. A red filter (590-nm cut-on) was used with the Xe lamp. The radiant intensity was measured with an E G & G (Salem, Mass.) Model 550 radiometer/photometer. To measure the real incident light intensity on the photoelectrode (without correction for solution absorbance) accurately, a diaphragm with a hole of area 0.020 cm^2 was attached to the detector of the radiometer. Neutral density filters were used to vary the intensity of the light.

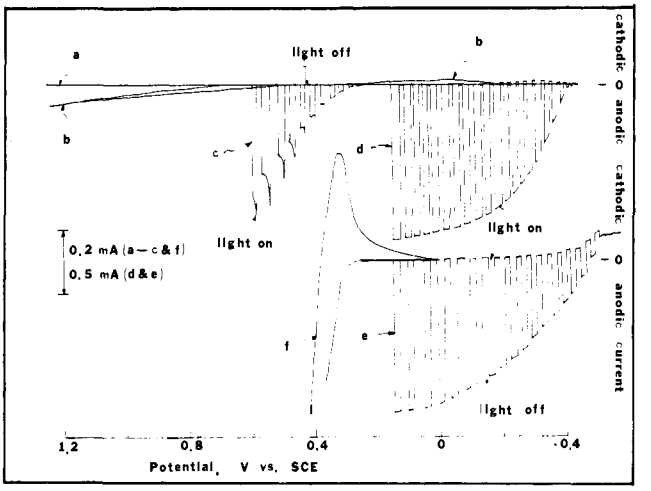

Figure 1. Voltammetric curves of n-WSe_2 and Pt in 0.50 M Na_2SO_4, scan rate 10 mV/s, light source 450-W Xe lamp with a 590-nm cut-on filter. (a) Dark cyclic voltammogram on n-WSe_2. No iodide or iodine in solution. (b) Dark cyclic voltammogram on n-WSe_2. Solution contained 1.0 M NaI. (c) Current–potential curve under illumination by chopped red light on n-WSe_2. No iodide or iodine in solution. (d) Current–potential curve under illumination by chopped red light on n-WSe_2. Solution contained 1.0 M NaI. (e) Same conditions as in (d) but solution contained 1.0 M NaI and 0.10 M iodine. (f) Cyclic voltammogram on Pt. Solution contained 0.10 M NaI. Initial potential at –0.10 V vs. SCE.

Reagent-grade chemicals were used without further purification. All solutions were prepared from triply distilled water and deoxygenated for at least 30 min with purified nitrogen before each experiment. All experiments were carried out with the solution under a nitrogen atmosphere.

Results

Electrochemical Behavior of n-WSe_2 in Iodide–Triiodide Solutions. The cyclic voltammetric behavior of iodide at n-WSe_2 and Pt electrodes is shown in Figure 1. Consider first the behavior of an n-WSe_2 electrode in a solution of 0.50 M Na_2SO_4 at pH 4.5 with and without 1.0 M NaI (curves a–d). In the absence of iodide in the dark a negligibly small background current was observed (curve a). In the presence of iodide, a slightly higher anodic background current, presumably due to the oxidation of iodide, and a reduction peak located at –0.05 V vs. SCE on scan reversal were found (curve b). The peak at –0.05 V was probably due to the reduction of the small amount of I_3^- generated during the anodic scan, since this peak was not seen when the potential was first scanned cathodically from an initial potential at 0.15 V vs. SCE. Under illumination with slowly chopped red light (wavelength ≥590 nm), an anodic photocurrent commencing at 0.30 V vs. SCE (curve c) was observed on n-WSe_2 electrodes in a solution of 0.50 M Na_2SO_4 at pH 4.5. No cathodic photocurrent was found, as expected, for the n-type material. In the presence of 1.0 M NaI, the onset photopotential, V_{on}, shifted to a much more negative potential, –0.45 V vs. SCE (curve d). This photocurrent can clearly be attributed to the oxidation of iodide and brownish red I_3^- is seen streaming from the n-WSe_2 electrode surface. Under a light intensity of ~150 mW/cm^2 for a solution containing 1.0 M I^-, the photocurrent was not limited by the mass transfer of iodide to the electrode surface, since it was unaffected by stirring and varied with light intensity. The addition of iodine (0.10 M) to the solution shifted V_{on} to slightly more negative potentials (~-0.50 V vs. SCE (curve e)). Note that the photocurrent for the oxidation of iodide on n-WSe_2 electrodes lies at potentials negative of the potentials for the iodide–triiodide couple

(2) (a) Tributsch, H.; Bennett, J. C. *J. Electroanal. Chem.* **1977**, *81*, 97. (b) Tributsch, H. *Ber. Bunsenges. Phys. Chem.* **1977**, *81*, 361. (c) *Ibid.* **1978**, *82*, 169. (d) *J. Electrochem. Soc.* **1978**, *125*, 1086. (e) Gobrecht, J.; Gerischer, H.; Tributsch, H. *Ibid.* **1978**, *125*, 2085. (f) Wrighton, M. S., private communication.

(3) Gobrecht, J.; Gerischer, H.; Tributsch, H. *Ber. Bunsenges. Phys. Chem.* **1978**, *82*, 1331.

(4) Tributsch, H.; Gerischer, H.; Clemen, C.; Bucher, E. *Ber. Bunsenges. Phys. Chem.* **1979**, *83*, 655.

(5) Nozik, A. J. *Appl. Phys. Lett.* **1977**, *30*, 567.

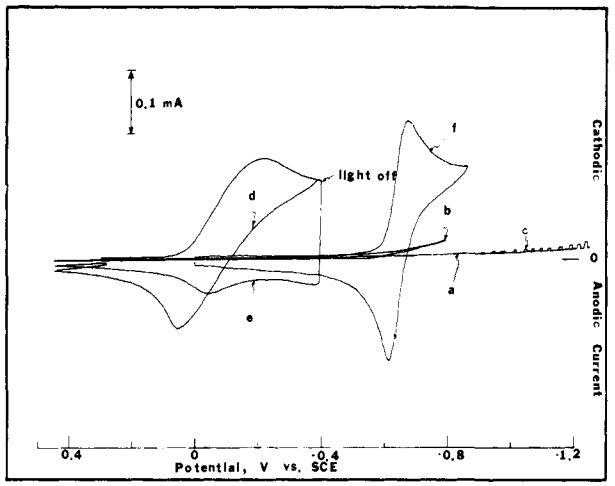

Figure 2. Voltammetric curves of p-WSe_2 in 1.0 M KCl solution, scan rate 50 mV/s, 450-W Xe lamp fitted with a 590-nm cut-on filter as the light source. (a) Dark voltammetric curve on p-WSe_2. No methylviologen in solution. (b) Same as curve (a) but solution contained 50 mM $MVCl_2$. (c) Current–potential curve under illumination by chopped red light on p-WSe_2. No methylviologen in solution. (d) Current–potential curve under illumination by red light on p-WSe_2. Solution contained 50 mM $MVCl_2$. (e) Same conditions as curve (d) but light was off during the back scan. (f) Cyclic voltammogram on Au. Solution contained 50 mM $MVCl_2$.

on Pt electrodes, V_{redox} (curve f); this potential difference represents the conversion of light to electrical energy. From the current-voltage curves on Pt and n-WSe_2 one predicts that a PEC cell based on n-WSe_2 and Pt electrodes in an I^-/I_3^- solution should have an open circuit potential of $V_{redox} - V_{on}$ (~0.7 V). The high light-limited current density found suggests a high quantum efficiency for I^- oxidation at the n-WSe_2, and that an efficient solar cell based on n-WSe_2 can be constructed. Such a cell is described below.

Electrochemical Behavior of p- and n-WSe_2 in Methylviologen Solutions. Cyclic voltammograms of methylviologen (*N,N'*-dimethyl-4,4'-bipyridinium, MV^{2+}) at p-WSe_2 and Au electrodes

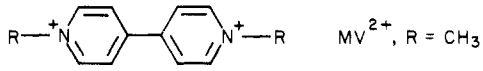

are shown in Figure 2. As shown in curve a, a negligibly small background current was observed at p-WSe_2 in the dark in the background electrolyte (1.0 M KCl) solution. In the presence of MV^{2+}, the cathodic background current was slightly higher (curve b), probably because of a small amount of reduction of MV^{2+}. In 0.1 M KCl, pH 4.5, without MV^{2+}, irradiation of p-WSe_2 electrodes with red light caused a significant cathodic current only at potentials negative of -1.0 V vs. SCE (curve c). In the presence of MV^{2+} a large increase in the cathodic photocurrent appeared at ~0.10 V vs. SCE (curve d). This photocurrent can clearly be attributed to the reduction of MV^{2+}, since the blue-purple $MV^{+\cdot}$ streamed from the surface of the p-WSe_2 electrode under these conditions. Upon scan reversal, the $MV^{+\cdot}$ was oxidized back to MV^{2+}. If the light was extinguished following the peak for the reduction of MV^{2+}, the current immediately dropped to anodic values and the anodic peak in the dark occurred at more positive potentials than it did under irradiation (curve e). As is clear from a comparison of curves d and f, the reduction of MV^{2+} takes place at irradiated p-WSe_2 at potentials significantly positive of the reversible $MV^{2+}/MV^{+\cdot}$ potential at Au. With the light intensity (~150 mW/cm^2) and the concentration of MV^{2+} (~50 mM) used in the described experiments, the photoreduction current on p-WSe_2 was limited by the rate of diffusion of MV^{2+} to the electrode surface, since the cathodic peak potential (i_{pc}) was proportional to the square root of the scan rate. An "underpotential" of 0.75 V can be achieved. The cyclic voltammetric results suggest that a PEC cell based on p-WSe_2 and Au electrodes in a $MV^{2+}/MV^{+\cdot}$ solution should show a fairly good efficiency.

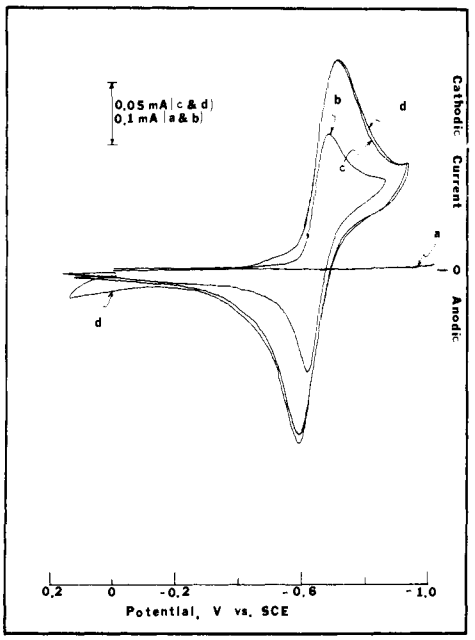

Figure 3. Voltammetric curves of n-WSe_2 and Pt in 1.0 M KCl solution, scan rate 50 mV/s, 450-W Xe lamp fitted with a 590-nm cut-on filter as the light source. (a) Dark cyclic voltammetric curve on n-WSe_2. No methylviologen in solution. (b) Cyclic voltammograms on Pt. Solution contained 50 mM $MVCl_2$. (c) Dark cyclic voltammogram on n-WSe_2. Same solution as in (b). (d) Current–potential curve under illumination by red light on n-WSe_2. Same solution as in (b).

The cyclic voltammetric behavior of MV^{2+} at n-WSe_2 is shown in Figure 3. In a 1.0 M KCl solution without MV^{2+}, a negligibly small background current was observed (curve a). In the presence of MV^{2+}, a reversible cyclic voltammogram is found at n-WSe_2 in the dark, which is similar to that found with Pt (see curves b and c); this can clearly be attributed to the redox reactions of the methylviologen species. Irradiation of the electrode showed no effect on either the reduction of MV^{2+} or the reoxidation of $MV^{+\cdot}$ (curve d).

Electrochemical Behavior of n-WSe_2 with Other Redox Systems. The photooxidation of several other couples with standard potentials ranging from -0.45 to 1.12 V vs. SCE were also investigated on n-WSe_2. For the heptylviologen couple ($HV^{2+}/HV^{+\cdot}$) (standard potential, V° = -0.49 V vs. SCE), a reversible cyclic voltammogram similar to that on Pt was observed in the dark. No photoeffect was observed. The behavior of this and several other systems at n-WSe_2 is illustrated in Figure 4. The onset photopotentials, V_{on}, for the redox reactions with $-0.45\ V < V^\circ \lesssim 0.55$ V vs. SCE are nearly independent of the redox couples used in this study; for example, Fe(II)–EDTA, $Fe(CN)_6^{4-}$, and I^- all show V_{on} ~0.40 V vs. SCE. The reduction of the photooxidized species for these compounds occurred only at potentials more negative than 0 V vs. SCE. For redox couples with $0.55\ V < V^\circ < 1.0$ V vs. SCE, the V_{on} depended strongly on the particular species. V_{on} ranged from ~0.15 V for Fe(II) to ~0.10 V for Br^-, and was ~0.30 V for background oxidation. The reduction of the photogenerated bromine began at quite positive potentials, ~0.6 V vs. SCE. The photooxidation of compounds with V° more positive than that for water oxidation is uncertain because of the background photoreaction. Actually, V_{on} for a 0.5 M H_2SO_4–0.5 M Na_2SO_4 solution was essentially the same in the absence and presence of chloride (see curves 7 and 8). The results for n-WSe_2 are summarized in Table I.

Photovoltaic (Solar) Cell Measurements. Regenerative semiconductor/liquid junction solar cells were fabricated by immersing the semiconductor electrode and a suitable counterelectrode in an aqueous solution containing the appropriate redox couple.

(a) The n-WSe_2/Iodide,Triiodide/Pt System. Photovoltaic cells were set up with an n-WSe_2 photoanode and a platinum foil cathode immersed in a solution containing 1.0 M I^-, 0.025 M I_3^-, and 1.0 M H^+. The action spectrum of the short-circuit photo-

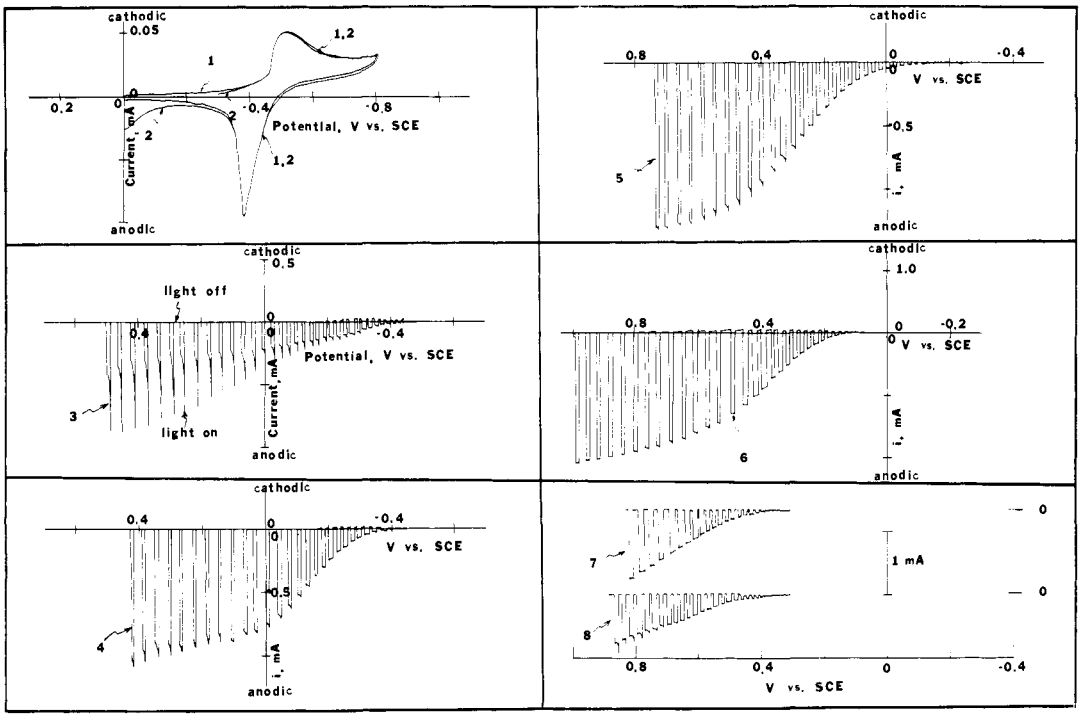

Figure 4. Current-potential curves of n-WSe_2 in various electrolyte solutions, 450-W Xe lamp fitted with a 590-nm cut-on filter as the light source. (1) Dark cyclic voltammogram in solution containing 0.2 M KBr and 10 mM heptylviologen bromide. (2) Voltammogram under illumination by red light. Same solution as in (1). (3) Current-potential curve under chopped red light in a solution containing 0.50 M Na_2SO_4 and 0.10 M Fe(II)-EDTA. (4) Current-potential curve under chopped red light in a solution containing 0.50 M Na_2SO_4 and 0.60 M $K_4Fe(CN)_6$. (5) Current-potential curve under chopped red light in a solution containing 0.50 M Na_2SO_4, 0.50 M H_2SO_4, and 0.50 M $FeSO_4$. (6) Current-potential curve under chopped red light in a solution containing 0.50 M Na_2SO_4, 0.50 M H_2SO_4, and 1.0 M KBr. (7) Same as in (6) but solution contained only 0.50 M Na_2SO_4 and 0.50 M H_2SO_4. (8) Current-potential curve under chopped red light in a solution containing 0.50 M Na_2SO_4, 0.50 M H_2SO_4, and 1 M KCl.

Table I. Voltammetric Data, Onset Photopotential,[a] and "Underpotential" at n-WSe_2

redox couple	V°, V vs. SCE[b]	V_{on}, V vs. SCE	underpotential $\Delta V = V_{on} - V^\circ$, V	theoretical underpotential[e] $\Delta V = V_{fb} - V^\circ$, V
Cl^-/Cl_2 (pH 0)	1.12			1.57
H_2O/O_2 (pH 0)	0.99	0.30	0.69	1.44
Br^-/Br_2 (pH 0)	0.82	0.10	0.68	1.27
Fe(II)/Fe(III) (1 N H_2SO_4)	0.53	−0.15	0.68	0.77
I^-/I_2 (pH 0)	0.29	−0.45	0.74	0.74
$Fe(CN)_6^{4-}/Fe(CN)_6^{3-}$ (pH 6)	0.22	−0.40	0.62	0.67
Fe(II)-EDTA/Fe(III)-EDTA (pH 5)	−0.15	−0.45	0.30	0.30
$HV^{+\cdot}/HV^{2+}$ (pH 5)[c]	−0.48	no photoeffect		
$MV^{+\cdot}/MV^{2+}$ (pH 2.5)[d]	−0.66	no photoeffect		

[a] The onset photopotential V_{on} here is defined as the potential at which 1% of the limiting or maximal photocurrent is observed. [b] V° = the standard potential. [c] HV = heptylviologen (1,1'-diheptyl-4,4'-bipyridyl). [d] MV = methylviologen (1,1'-dimethyl-4,4'-bipyridyl). [e] V_{fb} is taken as −0.45 V vs. SCE.

current, i_{ss}, is shown in Figure 5. It has been corrected for the solution absorbance and the output of the monochromator. It corresponds well to the literature absorption spectrum of WSe_2[6] at longer wavelengths. At shorter wavelengths, the photocurrent decreases with wavelength, suggesting that the photoeffect is due to a d–d electron transition.[3] The band gap of WSe_2 was estimated to be 1.4 eV from the "tail" of the photocurrent action spectrum. The i–V characteristic of this cell under irradiation of 150 mW/cm^2 yields a fill factor of 0.46. The open-circuit photovoltage approached a saturation value of 0.72 V at light intensities $\gtrsim$10 mW/cm^2. The short-circuit photocurrent did not show any signs of saturation at light intensities up to ~150 mW/cm^2.[18]

Irradiation of the n-WSe_2 crystal with the full visible (longer than 590 nm and IR filtered) output (150 mW/cm^2) from a 450-W Xe lamp focused onto the photoelectrode surface yielded a constant short-circuit photocurrent ~65 mA/cm^2 and an open-circuit photovoltage ~0.71 V. The maximum power effi-

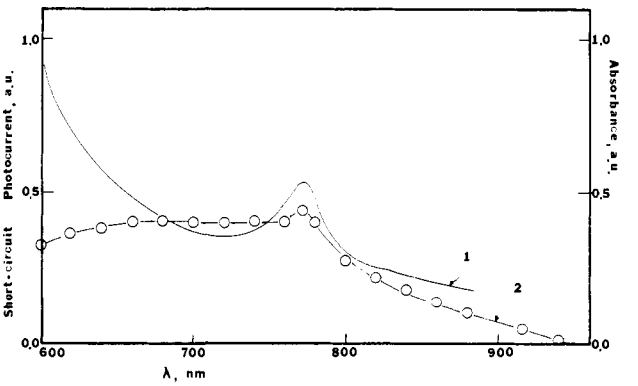

Figure 5. Action spectrum of the short-circuit photocurrent for a n-WSe_2/1.0 M NaI,0.05 M I_2/Pt solar cell (curve 2) and the absorption spectrum of WSe_2 (curve 1). The photocurrent action spectrum has been corrected for the solution absorbance and the output of the monochromator.

(6) Frindt, R. F. *J. Phys. Chem. Solids* **1963**, *24*, 1107.

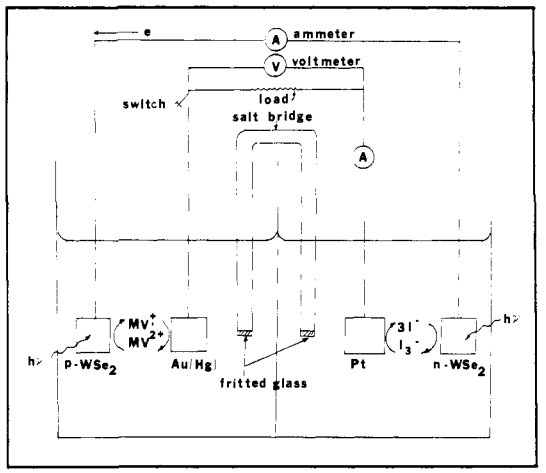

Figure 6. Schematic representation of a rechargeable PEC cell based on p-WSe_2/MV^{2+}/I^-/n-WSe_2 system.

ciency under these conditions was estimated as 14%. No attempts were made to minimize or correct for reflections at the cell window or electrode or the solution absorbance due to I_3^-; the optical path through the solution to the electrode was about 1 cm. After a total of 8 h of illumination, the current and voltage were essentially the same and the electrode surface showed no apparent change.

(b) The n-WSe_2/Bromide,Bromine/Pt System. When a solution containing 1.0 M Br^-, 0.02 M Br_2, and 1.0 M H^+ was used as the electrolyte, a lower fill factor (0.30) and a lower open-circuit photovoltage (0.61 V) were found, but the short-circuit photocurrent was higher (~85 mA/cm²) (compared to the I^-/I_3^- system). This higher short-circuit photocurrent is mainly caused by a lower absorbance of the Br^-/Br solution used. The maximum power efficiency with a light intensity of 150 mW/cm² was ~11%.

(c) The p-WSe_2/MV^{2+}/I^-/n-WSe_2 System: A Rechargeable Photoredox Cell. A rechargeable PEC cell is one which generates a photocurrent and at the same time carries out a photoelectrosynthetic reaction (i.e., generates species which can react spontaneously) so that the cell can be discharged in the dark with the production of a current flow opposite to that during the light-induced charging step. Such a cell resembles a storage battery, except that the charging is carried out by light rather than by an external power supply. Several types of rechargeable PEC cells have been discussed.[7] When all species in the cell are soluble, the cell is termed a rechargeable photoredox cell by analogy to redox storage cells. Rechargeable photocells based on methylviologen iodide, with p-WSe_2 as the photocathode, n-WSe_2 as the photoanode, and a pair of inert electrodes for the discharge step, were also investigated. The cell used in this preliminary study consisted of two compartments containing a common solution, 50 mM MV^{2+} and 1 M I^-, in which a p-WSe_2 and an n-WSe_2 electrode were immersed (see Figure 6). Both compartments were separated by a saturated KCl salt bridge. When the n- and p-type WSe_2 electrodes were illuminated simultaneously under short-circuit conditions, MV^{2+} was reduced to $MV^{+\cdot}$ at the p-WSe_2 and I^- was oxidized to I_2 (or I_3^-) at the n-WSe_2. The net reaction was

$$MV^{2+} + I^- \underset{\text{dark (discharge)}}{\overset{(+h\nu)\text{ light (charge)}}{\rightleftharpoons}} MV^{+\cdot} + {}^1/_2I_2 \qquad (1)$$

In this process radiant energy is converted into chemical energy (as $MV^{+\cdot}$ and I_2) which can be stored and converted into electrical energy by the corresponding back-reactions via the pair of inert electrodes. Pt and amalgamated Au were used here as the inert electrodes to avoid the overpotentials associated with the reduction of I_2 at p-WSe_2 and for the oxidation of $MV^{+\cdot}$ at n-WSe_2. Amalgamated Au (rather than Pt) was used as the second electrode in the compartment containing the p-WSe_2 electrode to prevent the Pt-catalyzed reaction of $MV^{+\cdot}$ with protons which produces hydrogen.

(7) (a) Hardee, K. L.; Bard, A. J. *J. Electrochem. Soc.* **1977**, *124*, 215. (b) Manassen, J.; Hodes, G.; Cahen, D. *Ibid.* **1977**, *124*, 532. (c) Memming, R. *Philips Tech. Rev.* **1978**, *38*, 160.

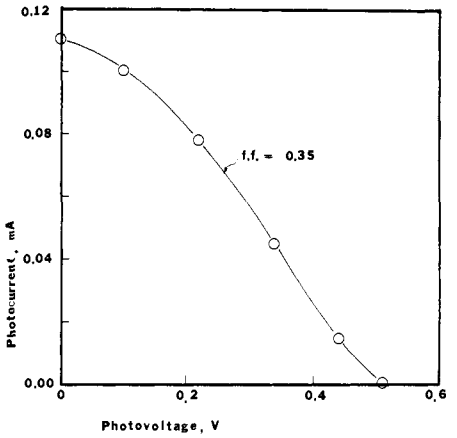

Figure 7. Photocurrent–photovoltage characteristic of a dual PEC cell based on p-WSe_2/50 mM MV^{2+}/1.0 M I^-/n-WSe_2 system; 450-W Xe lamp fitted with a 590 nm cut-on filter and a 1.6-mW He–Ne laser were used as the light sources.

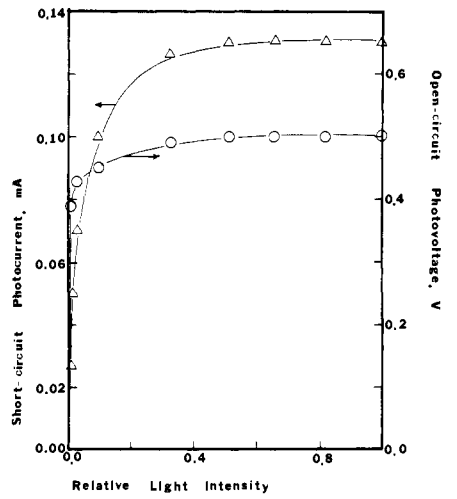

Figure 8. Open-circuit photovoltage and short-circuit photocurrent as functions of light intensity. A 450-W Xe lamp fitted with a 590-nm cut-on filter and a series of neutral density filters to vary the intensity was used to irradiate p-WSe_2 and a 1.6-mW He–Ne laser was used as a constant-intensity light source for n-WSe_2; p-WSe_2/50 mM MV^{2+}/1.0 M I^-/n-WSe_2.

As shown in Figure 7, the photocurrent–photovoltage characteristic of this cell yields a fill factor of 0.35 at a light intensity ~100 mW/cm². With this light intensity the short-circuit photocurrent was limited by the rate of mass transfer of MV^{2+} to the surface of p-WSe_2. The effect of light intensity on the open-circuit photovoltage (V_{oc}) and short-circuit photocurrent (i_{ss}) is shown in Figure 8. V_{oc} rises quickly to a saturation value of 0.50 V. The current shows a linear increase at low intensities, but then saturates when the mass transfer of MV^{2+} becomes important (i.e., when the light flux exceeds the flux of reactant, MV^{2+}, to the electrode surface). The maximum quantum efficiency of the system was estimated from the slope of the linear portion of the i_{ss} vs. light intensity curve. Since a dual photocell, i.e., one composed of two well-matched photoelectrodes, requires twice as many photons to generate a given photocurrent as compared to a single photoelectrode based cell, the p-WSe_2/n-WSe_2 based cell will have a quantum efficiency which is at most one-half that of either the n-WSe_2/iodide–triiodide cell or the p-WSe_2/methylviologen system (assuming low recombination rates in all cases). At a light intensity of ≲15 mW/cm², where the short-circuit photocurrent was not limited by the mass transfer effect, the quantum efficiency of the p-WSe_2/MV^{2+}/I^-/n-WSe_2 cell (electrons generated/total photons absorbed) was ~35% (short-circuit conditions).

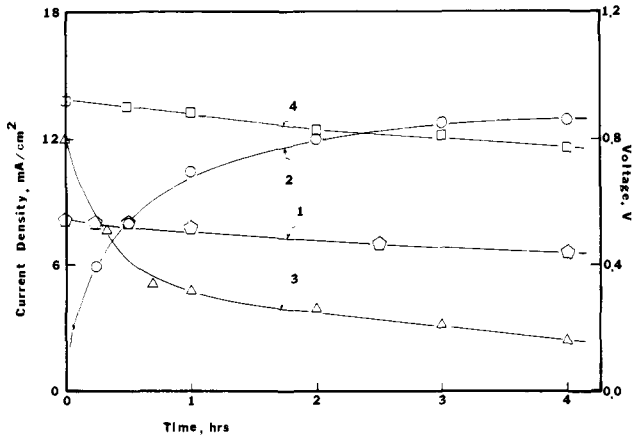

Figure 9. Charge–discharge time behavior of a rechargeable solar cell based on a system illustrated in Figure 8. Same light sources and solution as illustrated in Figure 8. (1) Short-circuit photocurrent during photocharging. (2) Open-circuit voltage across Au(Hg) and Pt during photocharging. (3) Discharge current after 4 h photocharging with short-circuit external load. Internal cell resistance ca. 1 kΩ. (4) Open-circuit voltage after photocharging on standing.

Figure 9 shows typical charge–discharge characteristics of the cell. Curve 1 represents the photocurrent during the charging process. The short-circuit photocurrent decreased slightly as the color of the solution became darker. During the charging process the open-circuit voltage between the Au(Hg) and Pt electrodes increased with time (curve 2). After 4 h of photocharging under short-circuit conditions (i.e., connected across milliammeter; passage of ~5.8 C), the cell was discharged under short-circuit conditions (curve 3). The origin of the discrepancy between the total charge generated in the photocharging and that passed in the discharging process is not clear but might involve the disproportionation of $MV^{+\cdot}$,[16] and the oxidation of $MV^{+\cdot}$ due to trace amounts of oxygen present in the cell. The time behavior of the open-circuit cell voltage after 4 h of photocharging is shown in curve 4; the slight decrease with time suggests that some leakage occurred in the system. The loss of $MV^{+\cdot}$ via side reactions was also indicated by the gradual buildup of brown triiodide in the compartment containing the n-WSe_2 electrode after several photocharge–discharge cycles.

It shoud be mentioned that rather preliminary results on n- and p-WSe_2 are presented here. Further investigations are necessary to elucidate details in their photoelectrochemical behavior and to test the possible utility of such systems.

Discussion

The n-WSe_2/Solution Interface. Three models have been proposed for a semiconductor/solution interface, i.e., the idealized,[8] recombinative,[9] and Fermi level pinning[10] models. The results given in Table I suggest that the simple idealized model does not account for the PEC behavior observed. For the ideal semiconductor/liquid junction, the onset photopotential, V_{on}, would be constant (near the flat-band potential, V_{fb}) and the photopotential, ΔV_{ph}, would be given by $\Delta V_{ph} \sim |V_{fb} - V^{\circ}|$ and thus would vary linearly with the standard potential, V°, of the redox couple with a unit slope. The results in the last two columns of Table I show that such behavior is followed for the more negative couples ($V^{\circ} < 0.3$ V vs. SCE), but not for the others. In the Fermi level pinning model,[10] the extent of the semiconductor band bending is limited by a relatively high density of surface states with energies within the band gap, and leads to ΔV_{ph} values that are almost independent of V°; such behavior has been observed for p-GaAs[10c] and p-Si.[10b] This model is not unambiguously supported by the present results, since V_{on} is nearly constant and the underpotential changes with V° for the couples with $-0.45 < V^{\circ} < 0.29$ V vs. SCE. The recombinative model is consistent with the PEC behavior observed and is described in more detail below.

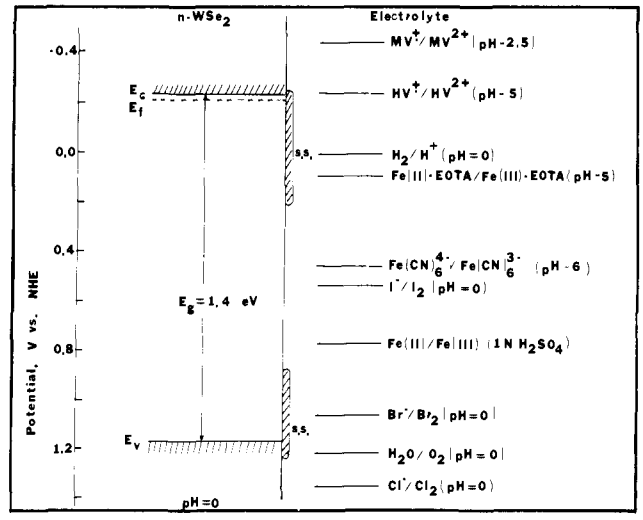

Figure 10. Schematic representation of the energetic situation at the n-WSe_2/solution interface. E_c = conduction band edge; E_f = Fermi energy corresponding to flat-band potential; E_v = valence band edge; E_g = band gap; s.s. = surface states.

As shown in Table I, the most negative value of V_{on} at n-WSe_2 is –0.45 V vs. SCE. This value was essentially independent of the V° of the redox couple (for I^-/I_2, $Fe(CN)_6^{4-/3-}$, and Fe(II)–EDTA/Fe(III)–EDTA). For redox couples with V° more negative than –0.45 V (i.e., the $HV^{+\cdot}/HV^{2+}$ and $MV^{+\cdot}/MV^{2+}$ couples), reversible charge transfer reactions occurred in the dark (Figure 4) and no photoeffect was observed. These results suggest that V_{fb} of n-WSe_2 is ~–0.45 V vs. SCE, which is close to that determined from the capacitance measurements.[11]

Dark reduction on n-WSe_2 of the oxidized form of redox couples with $-0.45 \leq V^{\circ} \leq 0.55$ V vs. SCE begins at potentials negative of 0 V vs. SCE, while the reduction of the photogenerated bromine occurs at ~0.6 V vs. SCE (Figure 4). These dark reductions at potentials positive of the conduction band edge have been attributed to charge transfer via surface states or intermediate levels in the gap region.[9] However, we should note that for the redox couples with V° more negative than 0.6 V vs. SCE (e.g., Fe^{3+}/Fe^{2+}, I_2/I^-), the dark reduction did not occur until significantly more negative potentials. This suggests that there is a window ranging from 0 to ~0.6 V in the gap region in which surface states are apparently absent, or perhaps that Br^-/Br_2 interacts strongly with the electrode surface altering the band structure and surface levels. A schematic representation of the energetic situation at the n-WSe_2/solution interface, neglecting the band bending but including the surface states under the assumption of no specific surface interactions, is shown in Figure 10. As suggested from this figure, the loss of the photogenerated species via surface recombination is probably higher for Br^-/Br_2 than for I^-/I_2, since the reduction of Br_2 can take place either through the higher or through the lower surface states, whereas the back electron transfer from the semiconductor to I_2 can only take place through the higher ones. This recombination leads to an apparent positive shift in V_{on} and hence to a degradation in the open-circuit photovoltage. The detailed characteristics of p-WSe_2 and other layer-type materials will be discussed in a separate paper.

Photovoltaic Cells Based on n-WSe_2 Electrodes. The open-circuit photovoltage of the two electrode photovoltaic cells, V_{oc}, should ideally approach the theoretical value of ΔV_{ph} given in Table I. The n-WSe_2/I^-,I_2/Pt system shows a V_{oc} of 0.71 V, which is very close to the predicted value of 0.74 V. For the n-WSe_2/Br^-,Br_2/Pt system, however, the V_{oc} of 0.61 V was sig-

(8) Gerischer, H. "Physical Chemistry: An Advanced Treatise"; Eyring, H., Henderson, D., Jost, W., Eds.; Academic Press: New York, 1970; Vol. 9A.

(9) Frank, S. N.; Bard, A. J. *J. Am. Chem. Soc.* **1975**, *97*, 7427.

(10) (a) Bard, A. J.; Bocarsly, A. B.; Fan, F.-R.; Walton, E. G.; Wrighton, M. S. *J. Am. Chem. Soc.*, in press. (b) Bocarsly, A. B.; Bookbinder, D. C.; Dominey, R. N.; Lewis, N. S.; Wrighton, M. S. *Ibid.*, in press. (c) Fan, F.-R.; Bard, A. J. *Ibid.*, in press.

(11) White, H. S.; Fan, F.-R.; Bard, A. J., unpublished results.

nificantly smaller than ΔV_{ph} (1.27 V). This difference can be attributed to the significant dark cathodic current which is present in the potential region far positive of the flat-band potential, leading to recombination as discussed in the preceding section. Along with this striking difference in V_{oc} between I^-/I_2 and Br^-/Br_2 systems, the fill factors for these two systems were also quite different. All of the factors which cause different fill factors for different redox couples with a given electrode are still not clear but probably also involve different recombination kinetics.

Photoassisted Hydrogen Evolution with the n-WSe_2/MV^{2+},I^-/p-WSe_2 System. It has been demonstrated that $MV^{+\cdot}$ can reduce water to produce hydrogen in the presence of a suitable heterogeneous catalyst:[12]

$$2MV^{+\cdot} + H_2O \xrightarrow{Pt} H_2 + 2OH^- + 2MV^{2+} \quad (2)$$

The photoreduction of water directly at small band gap p-type semiconductor electrodes is slow and inefficient, because these materials have high hydrogen overpotentials. We[13] and Wrighton et al.[14] have recently demonstrated the photoreduction of MV^{2+} at p-GaAs and p-Si; the subsequent generation of hydrogen in the p-GaAs cell as shown in eq 1 was also demonstrated.[13] However, these small band gap materials do not provide holes in the valence band with sufficiently positive potentials to oxidize water. Thus the photoreduction of MV^{2+} in a p-GaAs/metal cell can only be carried out by applying an external voltage to the electrodes.

As shown in Figure 2, the photoreduction of MV^{2+} on p-WSe_2 commences at ~0.10 V vs. SCE. Although this represents an "underpotential" of ~0.5 V, the photoreaction does not provide holes with sufficiently positive potentials to oxidize water or even iodide. Similarly, as shown in Figure 1, the photooxidation of I^- at n-WSe_2 cannot occur with the accompanying reduction of MV^{2+} on Pt, since the V_{on} of −0.45 V vs. SCE of n-WSe_2 is more positive than V° of the $MV^{2+}/MV^{+\cdot}$ couple. However, the combination of an n- and a p-WSe_2 electrode can provide an efficient photoelectrode couple to photooxidize iodide on n-WSe_2 and simultaneously photoreduce MV^{2+} on p-WSe_2 without requiring an external power source. The excellent match of the onset photopotential, the nearly ideal band gap for the solar spectrum, and the high stability of the WSe_2 electrodes make the n-WSe_2/I^-/MV^{2+}/p-WSe_2 system a useful one in a path toward the photodecomposition of H_2O with semiconductor electrodes. However, the overall reaction carried out to produce H_2 and I_3^- is still only part of the way toward the water decomposition reaction and an additional process is needed for the reduction of iodine and oxidation of water to oxygen (e.g., in another PEC cell).

As concerns the hydrogen production reaction via the p-WSe_2/MV^{2+} half-cell, the catalytic reduction of water by $MV^{+\cdot}$ with a colloidal Pt–poly(vinyl alcohol) catalyst is perhaps sufficiently fast (rate constant of 5.7×10^4 s^{-1} with a Pt content of 1.25 mM[12c]) to keep the concentration of $MV^{+\cdot}$ sufficiently small to prevent the disproportionation or dimerization of $MV^{+\cdot}$. However, the application of the n-WSe_2/I^-/MV^{2+}/p-WSe_2 system as a rechargeable photobattery needs further investigation. The solubilities of MV^{2+} and $MV^{+\cdot}$ and the stability of $MV^{+\cdot}$ seem to be the key problems.

Conclusions

The results presented here with n- and p-WSe_2 electrodes suggest that these materials can be used in the construction of stable and efficient PEC cells. These findings confirm the prediction of Tributsch et al.[2-4] about the applicability of layer-type semiconductors for these purposes. We have demonstrated here several types of cells including photovoltaic (regenerative) ones, a photochargeable cell, and a cell suitable for the production of hydrogen. The practical application of such semiconductor devices will almost certainly require the use of polycrystalline materials or thin layers of materials. Electrodes produced from polycrystalline materials (e.g., sintered disks, deposited films) have been used with other semiconductors, such as TiO_2 and CdS, but these might be less applicable with WSe_2 and other layered compounds. We have found significant sample-to-sample variations in the properties of WSe_2 crystals and also found that the behavior and efficiency of these materials are strongly dependent upon the nature of the electrode surface. Indeed a recent study of the effect of crystal orientation on the behavior of layer compound electrodes showed that only the $\perp c$ surface is efficient for photoprocesses.[15-17] Work on oriented polycrystalline materials and epitaxial layers of WSe_2 is in progress.

Acknowledgments. This work was supported in part by the Office of Naval Research and by the Solar Energy Research Institute (in a cooperative project with SumX Corp.).

(12) (a) Lehn, J.-M.; Sanvage, J.-P. *Nouveau J. Chim.* **1977**, *1*, 449. (b) Krasna, A. I. *Photochem. Photobiol.* **1979**, *29*, 267. (c) Kiwi, J.; Gratzel, M. *Nature (London)* **1979**, *281*, 657.

(13) Fan, F.-R. F.; Reichman, B.; Bard, A. J. *J. Am. Chem. Soc.* **1980**, *102*, 1488.

(14) Bookbinder, D. C.; Lewis, N. S.; Bradley, M. G.; Bocarsly, A. B.; Wrighton, M. S. *J. Am. Chem. Soc.* **1979**, *101*, 7721.

(15) Kautek, W.; Gerischer, H.; Tributsch, H. *Ber. Bunsenges. Phys. Chem.* **1979**, *83*, 1000.

(16) Lewerenz, H. J.; Heller, A.; DiSalvo, F. J. *J. Am. Chem. Soc.* **1980**, *102*, 1877.

(17) Menezes, S.; DiSalvo, F. J.; Miller, B. *J. Electrochem. Soc.*, in press.

(18) The performance parameters of this all have been published. See: Fan, F.-R. F.; White, H. S.; Wheeler, B.; Bard, A. J. *J. Electrochem. Soc.* **1980**, *127*, 518.